Cement and Concrete Research 151 (2022) 106647

Contents lists available at ScienceDirect

Cement and Concrete Research

journal homepage: www.elsevier.com/locate/cemconres

Hydration kinetics of ternary slag-limestone cements: Impact of water to binder ratio and curing temperature

Ruben Snellings [a,*], Alisa Machner [b,e], Gerd Bolte [c], Hadi Kamyab [a], Pawel Durdzinski [c], Priscilla Teck [a,d], Maciej Zajac [c], Arnaud Muller [c], Klaartje de Weerdt [b], Mohsen Ben Haha [c]

[a] Unit Sustainable Materials, VITO, Belgium
[b] Dept. of Structural Engineering, NTNU, Norway
[c] Global R&D, HeidelbergCement, Germany
[d] Dept. Earth and Environmental Sciences, KULeuven, Belgium
[e] Dept. Civil, Geo and Environmental Engineering, TUMunich, Germany

ARTICLE INFO

Keywords:
Hydration
Composite cement
Slag
Limestone
Temperature
Water to binder ratio

ABSTRACT

Ternary cements are a promising option to further reduce CO_2 emissions and environmental impact from cement production. The current study investigates in detail the impact of water to binder ratio (0.4, 0.5, 0.6) and curing temperature (5, 20, 40 °C) on the hydration kinetics of a ternary cement comprising clinker, slag and limestone in a 50:40:10 mass ratio, respectively. The results show that the water to binder ratio mainly affected the hydration degree of slow reacting phases, such as slag and belite, at later ages. The curing temperature accelerated the hydration of alite to a lesser extent than that of C_3A and slag, which could lead to changes in the hydration reaction sequence at elevated curing temperatures. Elevated temperature curing did not lead to cross-over effects in terms of slag hydration degree at later ages but led to reductions in the portlandite and ettringite levels.

1. Introduction

Blended cements that contain ground granulated blast furnace slag (GGBFS) are known for their outstanding durability, long-term performance and low environmental footprint [1,2]. GGBFS is allocated only minor CO_2 emissions as a by-product of pig iron production, therefore clinker substitution by GGBFS is an effective and well-known means of reducing cement CO_2 footprint [3]. In consequence, there is a high demand for GGBFS among cement and concrete producers. However, GGBFS supply is constrained by production volumes of primary iron and steel, and the demand largely outstrips supply. Consequently, alternative supplementary cementitious materials (SCMs) are intensely sought for [4–6]. Another approach is to introduce a third cement constituent, such as limestone or coal combustion fly ash, to partially substitute GGBFS, while maintaining the high clinker replacement levels typical for GGBFS cements. These so-called ternary composite cements aim to make more efficient use of the available GGBFS resources without compromising cement and concrete performance [7]. This enables cement and concrete producers to extend their portfolio of low-clinker cements and further reduce average clinker factors of their products.

Characteristic for GGBFS and most SCM blended cements is the lower compressive strength development at early ages compared to neat Portland cement, e.g. CEM I [3]. This is mainly attributed to slower SCM reaction kinetics compared to alite (C_3S) [8]. Previous research concluded that GGBFS reactivity depends on the one hand on GGBFS intrinsic properties such as chemical composition [9–13], degree of crystallinity and fineness [14,15]. On the other hand the GGBFS reaction rate is affected directly by the reaction environment, i.e. the cement pore solution composition (pH) [16–18], the water to binder ratio [11,19] and the curing temperature [19–21], and indirectly by the cement formulation, i.e. the clinker replacement rate [11,22–24], the clinker composition [11,12] and the dosage of other constituents such as calcium sulfates or limestone [23,25,26]. Increases in solution pH, water to binder ratio and curing temperature all enhance GGBFS reactivity, but should be balanced against potential negative influences on long term performance or durability. Increasing the slag replacement reduces slag reaction degrees, for instance Taylor et al. [24] report GGBFS degrees of reaction at 20 years of hydration of 68% and 36% for 50 and 90 wt% clinker replacement by GGBFS, respectively. This illustrates that the residual fraction of unreacted, unused GGBFS can be very significant.

* Corresponding author.
E-mail address: ruben.snellings@vito.be (R. Snellings).

https://doi.org/10.1016/j.cemconres.2021.106647
Received 26 July 2021; Received in revised form 18 October 2021; Accepted 21 October 2021
Available online 27 October 2021

Adjustment of the GGBFS content to enable it to reach a high degree of reaction is therefore a rational objective. It allows to increase cement resource efficiency and to abate GGBFS overdemand. Compared to other SCMs, GGBFS is quite reactive and could compete with clinker phases for water and space, thus causing slightly lower degrees of clinker reaction than more slowly reacting SCMs such as fly ash [27].

Recent research has demonstrated that ternary cements comprising clinker, limestone and Al-rich SCMs such as fly ash or calcined clay benefit from a carbo-aluminate reaction [28,29]. This reaction of limestone with C_3A or Al-rich SCMs shifts the aluminate hydrate phase assemblage towards monocarboaluminate instead of monosulfoaluminate. Due to the presence of Al-rich SCMs, more ettringite and therefore a higher volume of solids are obtained, in turn leading to better pore space filling and increased compressive strength [30–32]. In case of GGBFS, the carbo-aluminate reaction has been observed only to a lesser extent, mainly because a large part of the Al contained in the slag participates in the formation of hydrotalcite-like phases [25,33]. However, the reactivity of GGBFS was observed to increase in combination with limestone. This was tentatively related to lowered Al concentrations in the cement pore solution [25,34]. In addition to engaging in cement hydration reactions, limestone is also known to be an efficient filler that boosts the early hydration of clinker phases to a larger extent than aluminosilicate fillers [35,36]. Experimental observations and supporting microstructural modelling attributed the higher limestone filler effect to a higher nucleation density of cement hydrates at the limestone surface [35,37].

Previous hydration studies on GGBFS-limestone blended cements mainly documented the hydration kinetics and products of GGBFS-limestone cement for a fixed water to binder ratio and curing at room temperature [25,38]. Optimization of the performance of the ternary cement used in the current study was reported in [7].

This study contributes complementary data on the effect of water to binder ratio and curing temperature on the hydration kinetics and products of a GGBFS-limestone blended cement and of its individual components. The reported data, acquired with state-of-the-art direct methods, can be used to parameterize or validate multiphase kinetic hydration models (e.g. [39–42]) that predict the development of concrete properties for GGBFS-limestone blended cements.

2. Materials and methods

2.1. Approach

The cement hydration kinetics were studied on pastes of the ternary GGBFS-limestone cement and a reference neat Portland cement. Various water to binder ratios (0.4, 0.5 and 0.6) and curing temperatures (5, 20 and 40 °C) were chosen to cover ranges representative of common practice. The degree of reaction of the clinker and GGBFS components was determined at 1, 2, 7, 28, 90 and 180 days of hydration using a combination of X-ray diffraction (XRD), thermogravimetric analysis (TGA) and scanning electron microscopy (SEM). At the same ages the cement hydrate assemblage was studied. The heat release of the hydrating cement pastes was followed continuously by isothermal calorimetry measurements until 28 days after mixing with water. The obtained data are used to derive the kinetic dependence on temperature (apparent activation energy) and water to binder ratio, both for individual components as for the composite multiphase cement. Descriptions of the cement microstructure and performance for varying water to binder ratio and curing temperature will be investigated in a follow-up study.

2.2. Materials

2.2.1. Cement constituent properties

The ternary cement consisted of a blend of 50 wt% Portland cement (PC; type CEM I 52.5 R according to EN 197-1:2011), 40 wt% of ground granulated blast furnace slag (S) and 10 wt% of limestone (L). The ternary cement (PC50S40L10) was optimized for performance by separate grinding of the constituents to specified fineness and subsequently blending the constituents together [7]. The particle size distribution of each cement constituent is given in Fig. 1. To meet early age

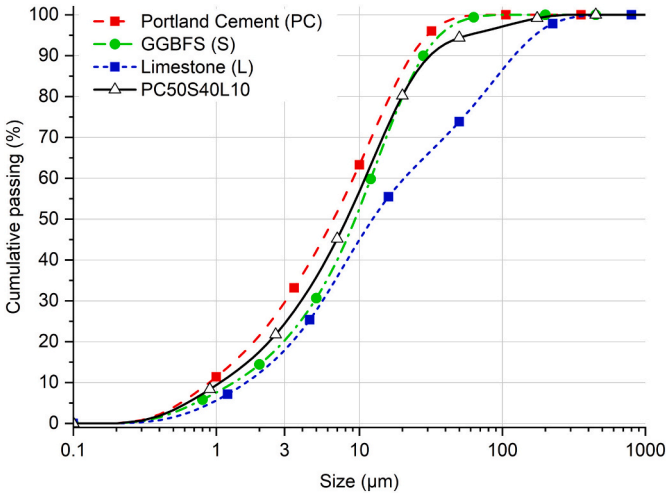

Fig. 1. Cumulative particle size distribution of the cement constituents and the resulting ternary blended cement (PC50S40L10).

Table 1
Physical and chemical properties of the ternary cement constituents.

Oxide (wt%)	PC	GGBFS	Limestone
Chemical composition			
SiO_2	20.35	35.21	0.85
Al_2O_3	5.46	11.27	0.15
TiO_2	0.28	1.07	0.01
MnO	0.04	0.21	0.06
Fe_2O_3	2.40	0.26	0.16
CaO	62.33	41.64	54.54
MgO	1.49	5.96	0.91
K_2O	0.89	0.64	0.04
Na_2O	0.20	0.22	0.01
SO_3	3.68	–	0.01
P_2O_5	0.12	0.01	0.01
LOI[a]	1.87	(+0.16)	43.32
Total	99.11	96.49	100.07
Physical properties			
BET (m^2/g)	1.90	2.61	1.10
Specific gravity (g/cm^3)	3.12	2.89	2.72
Blaine (cm^2/g)	5400	5010	3430
Phase composition			
Alite	62.2	–	–
Belite	11.2	–	–
C_3A ortho	4.2	–	–
C_3A cubic	6.5	–	–
C_4AF	5.6	–	–
Free Lime	–	–	–
Periclase	0.4	–	–
Gypsum	0.3	–	–
Bassanite	3.6	–	–
Anhydrite	1.8	–	–
Arcanite	1.4	–	–
Aphtitalite	0.2	–	–
Calcite	1.6	3.6	96.9
Quartz	1.2	0.9	0.7
Portlandite	0.7	–	–
Dolomite	–	–	2.4
Amorphous	–	95.5	–

[a] Loss On Ignition: measured by heating to 1050 °C for all constituents except GGBFS, which was heated to 950 °C. The GGBFS LOI weight gain is attributed to oxidation, and therefore reported within parentheses.

strength specifications, a fine industrial PC was used. Limestone as least reactive constituent was kept coarsest, GGBFS was positioned in between. Separate grinding provides better control on constituent particle size than intergrinding. In interground cements, softer constituents such as limestone will end up finer than the harder constituents and therefore may generate a different filler effect.

Other physical properties of the cement constituents, i.e. the BET specific surface area, the specific gravity and the Blaine fineness are presented in Table 1, together with the chemical composition determined by XRF and LOI and the phase composition as measured by XRD-Rietveld analysis.

2.2.2. Sample preparation

Paste samples were prepared for all combinations of water to binder (i.e. PC + slag + limestone) ratio (0.4, 0.5 and 0.6) and curing temperatures (5, 20 and 40 °C). The anhydrous cements and the mixing water were equilibrated overnight at the selected curing temperature. The mixing and casting of the paste samples were carried out at 20 °C. After adding the cement to the required amount of water, the mixture was gently homogenized with a spatula for 1 min before it was mixed with an overhead high-shear mixer for 2 min at 1600 rpm. Isothermal calorimetry specimens were immediately after mixing poured into the calorimeter glass ampoules. The ampoules were air-sealed and inserted in the calorimeter for measurement. Specimens for TGA, XRD and SEM analysis were cast into 12 mL HDPE tubes that were closed with a lid and sealed with parafilm. Samples were kept submerged in a water bath kept at constant temperature to secure isothermal conditions during curing. From each mixing, several tubes were filled with cement paste, so that for each testing age a separate specimen was available. The filled containers were stored under water at the respective curing temperatures until time of testing.

At the designated age of testing (1, 2, 7, 28, 90, and 180 days for the ternary cement; 7 and 90 days for the reference Portland cement) various discs were sawn from the specimen. The top and the bottom part of each specimen were discarded. 6 mm discs were cut from the specimens for analysis by TGA and XRD, which were coarsely crushed to <2 mm and the hydration was stopped by solvent exchange using isopropanol and petroleum or di-ethylether according to [43]. For SEM-EDS analysis, the 3 mm discs were cut, however they were not crushed but stored in 30 mL isopropanol for 7 days. Afterwards, the isopropanol was decanted, and the discs were dried in a desiccator above silica gel under low vacuum (−0.2 bar) for 2 days. All hydration-stopped samples were stored in the desiccator until further sample preparation and analysis.

An additional 3 mm disc was cut from the specimens, and was immediately measured by XRD after sawing without hydration stoppage. The disc was wet-polished briefly with distilled water on sandpaper to remove cutting traces and to obtain a flat surface for XRD measurement. Polishing residues were washed away with distilled water and the sample surface was superficially dried using dry compressed air.

2.3. Methods

The heat of hydration was measured by isothermal calorimetry to investigate the effect of water to binder ratio and curing temperature on the overall hydration kinetics of the blended cement. A TAM Air isothermal calorimeter placed in a constant temperature environment of 20 °C was used to measure the heat flow. For each measurement temperature (5, 20 and 40 °C), the calorimeter was recalibrated. As references, ampoules containing an amount of water matching the heat capacity of the paste samples were used. The heat flow baseline was measured when the signal stability reached below 250 nW/h and was then recorded for 180 min. The heat flow baseline was subtracted from the measurement signal when processing the data. The duration of the measurements was 28 days. The heat flow data were normalized to the initial PC content of each sample. The cumulative heat was obtained by integrating the normalized heat flow curve over time.

TGA was carried out on all samples after solvent exchange and grinding by hand to <63 μm, to determine their bound water and Ca$(OH)_2$ content. The mass loss of the samples was recorded over a temperature range of 40 to 900 °C using a Mettler Toledo DSC3+. A heating rate of 10 K/min was used, and the measurement cell was flushed with 50 mL/min nitrogen gas. The sample size was approximately 200 mg poured into 600 μL corundum crucibles. The bound water content was calculated based on the mass loss of the hydration stopped specimens between 50 and 550 °C. The mass loss related to the decomposition of Ca$(OH)_2$ was derived by integration of the Differential Thermogravimetric (DTG) curve over the 400 to 550 °C temperature interval with the subtraction of the background by a linear baseline as described in [44]. Both the bound water and the $Ca(OH)_2$ mass losses were normalized and reported to the sample mass at 550 °C, which was considered to be the dry binder mass that remains constant during cement hydration. Finally, the $Ca(OH)_2$ content and the bound water content were calculated and reported on dry binder or dry clinker mass basis.

XRD measurements were carried out, to obtain data on the reaction kinetics of individual cement components and to characterize the resulting hydration product assemblage. XRD measurements were made of both powdered hydration stopped samples and freshly polished discs. Measurements of hydration stopped samples were used to derive the degree of reaction of anhydrous cement phases. As hydration stoppage is known to affect the hydrate assemblage, the measurements of the fresh discs were used to follow the development of the cement hydration products.

Hydration stopped samples were hand ground to pass a 63 μm sieve immediately before the measurement. The powdered samples were back-loaded into the sample holders and measured one by one, to avoid carbonation due to exposure to ambient air during measurement. The hydration stopped samples were measured within 48 h after completing the solvent exchange procedure.

Freshly cut and polished discs were immediately mounted in the XRD sample holder. To obtain a level surface, each disc was positioned and fixed by modelling clay.

XRD measurements were made using a Panalytical Empyrean diffractometer. The diffractometer was equipped with a CoKα X-ray tube operated at 40 kV and 45 mA. The measurements were carried out in Bragg-Brentano configuration over an angular range of 5 to 90°2θ. The step size used was 0.013°2θ. A 2D solid state PIXcel^{3D} detector with 255 channels covering an active length of 3.35°2θ was used to record the diffracted X-ray intensity signal. The equivalent counting time per step was 50 s, corresponding to a total measurement duration of about 22 min per sample.

The XRD data were analyzed by Rietveld refinement to quantify the crystalline phase composition. Topas Academic v4.3 software was used for the analysis. The crystal structures used in the refinements were adopted from the list given by [45]. Lattice and peak shape parameters for the anhydrous phases were refined for the initial anhydrous cement constituents and kept constant in the Rietveld refinement of the hydrated cement samples. Lattice and peak shape parameters of the hydration products were refined for the hydrated samples to capture structural and textural changes during hydration. The external standard method as described by [46,47] was applied to account for amorphous or unidentified phases. The X-ray mass absorption coefficient used in the external standard method was calculated from the chemical composition of the cement and the remaining amount of water in the sample [48]. In case of the hydration-stopped sample, the bound water content measured by TGA was adopted, for the freshly cut discs the initial water to cement ratio was considered. To quantify the degree of reaction of the slag, a PONKCS phase [49] for the slag was integrated into the quantitative phase analysis following the procedure in [50]. The phase constant of the PONKCS phase was calibrated using anhydrous mixes of GGBFS and cement at known proportions. An additional peaks phase was introduced to account for the C-S-H signal. The C-S-H peaks phase

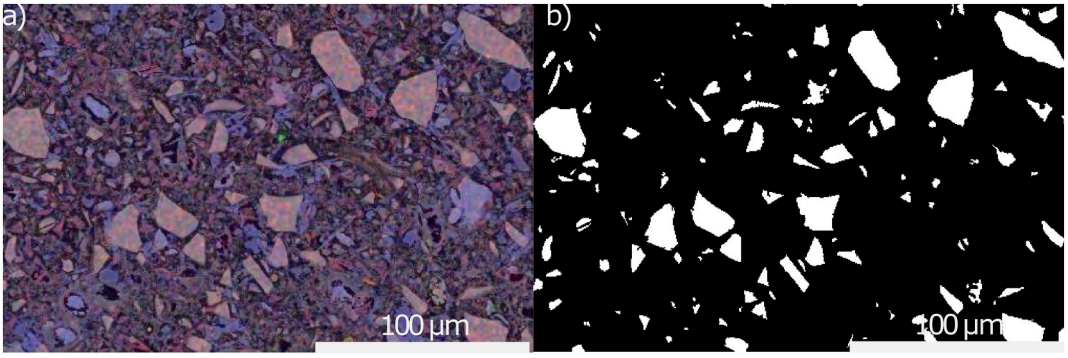

Fig. 2. Input and output of the image segmentation routine developed to recognize and quantify the fraction of slag particles in BSE-EDX images. a) Combined BSE-EDX image used as input, slag particles appear light pinkish, b) segmentation result, slag particles in white.

was modelled on corresponding cement samples stopped at 90 days of hydration by solvent exchange. Peak positions and shapes for the PONCKS and peaks phases were fixed during refinement of a series of hydrated samples. The quantification results were recalculated to the initial dry binder mass to enable comparison across samples.

Image analysis (IA) of scanning electron microscopy back-scattered electron (SEM BSE) images and energy dispersive X-ray (EDX) spectroscopic mappings was used as independent technique to validate the XRD analysis results on the degree of reaction of slag. For validation purposes, the BSE-EDX IA was carried out on a reduced set of samples, i.e. on a time series of the blended cement prepared at a water to binder ratio of 0.5 and cured at 20 °C and on all combinations of water to binder ratios and curing temperatures at the sample age of 28 days.

The hydration-stopped discs were vacuum impregnated in EPOFIX® epoxy resin. The epoxy resin was left to harden for 24 h at room temperature. The impregnated disc surface was stepwise polished down to 1 µm diamond grit size using an oil based lubricant to obtain a mirror surface appropriate for SEM-EDX measurements [51]. SEM-EDX data were acquired using a FEI FEG Nova NanoSEM 450 equipped with a Bruker XFlash 5030 detector. SEM BSE and EDX mappings were acquired at 500× magnification. The microscope was operated at an electron acceleration voltage of 20 kV and a working distance of 8.5 mm.

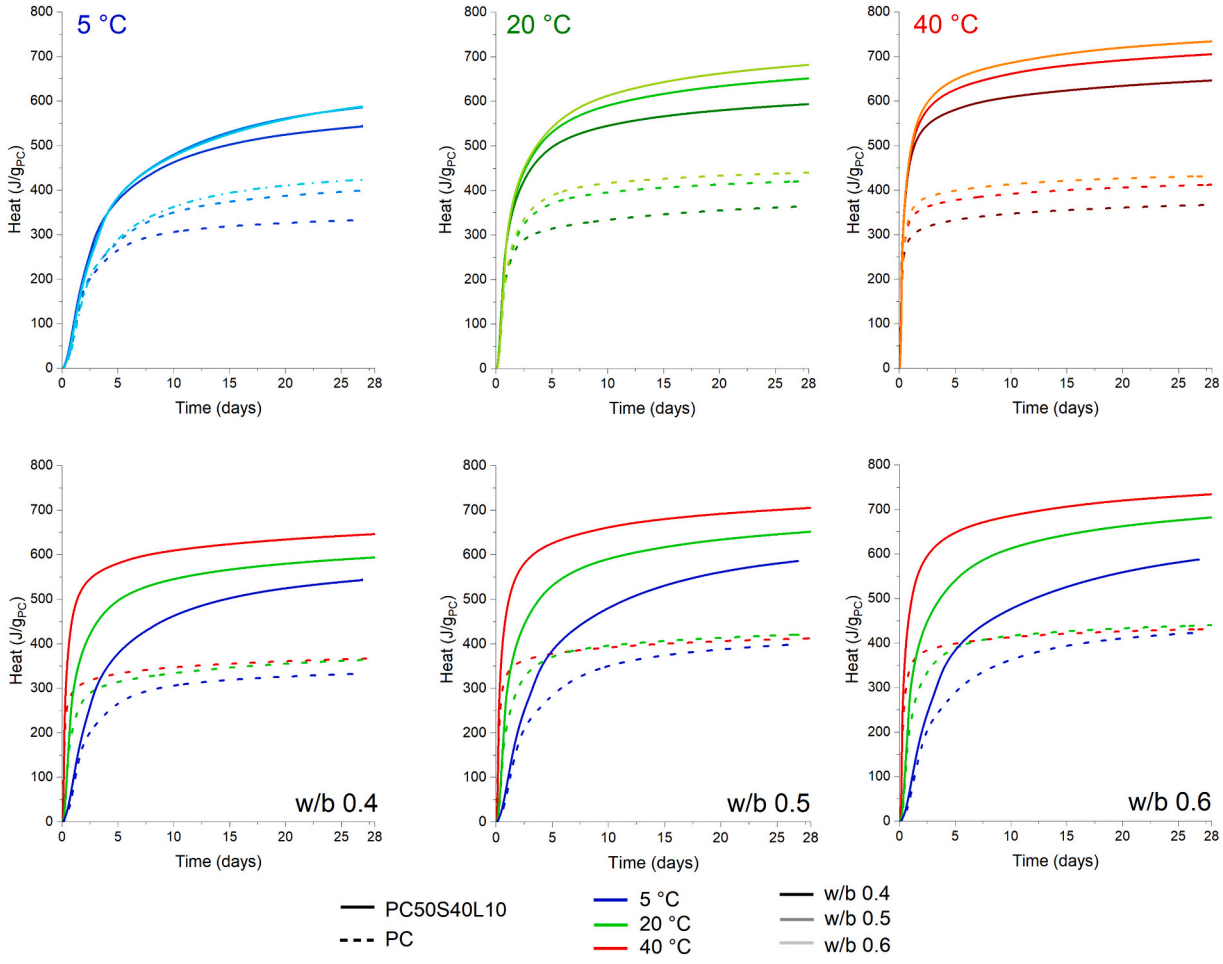

Fig. 3. Cumulative heat released during isothermal hydration of ternary slag-limestone cement (PC50S40L10) and reference neat Portland cement (PC) for water/binder mass ratios (w/b) of 0.4, 0.5 and 0.6 cured at 5, 20 and 40 °C. Results are reported to the mass of Portland cement.

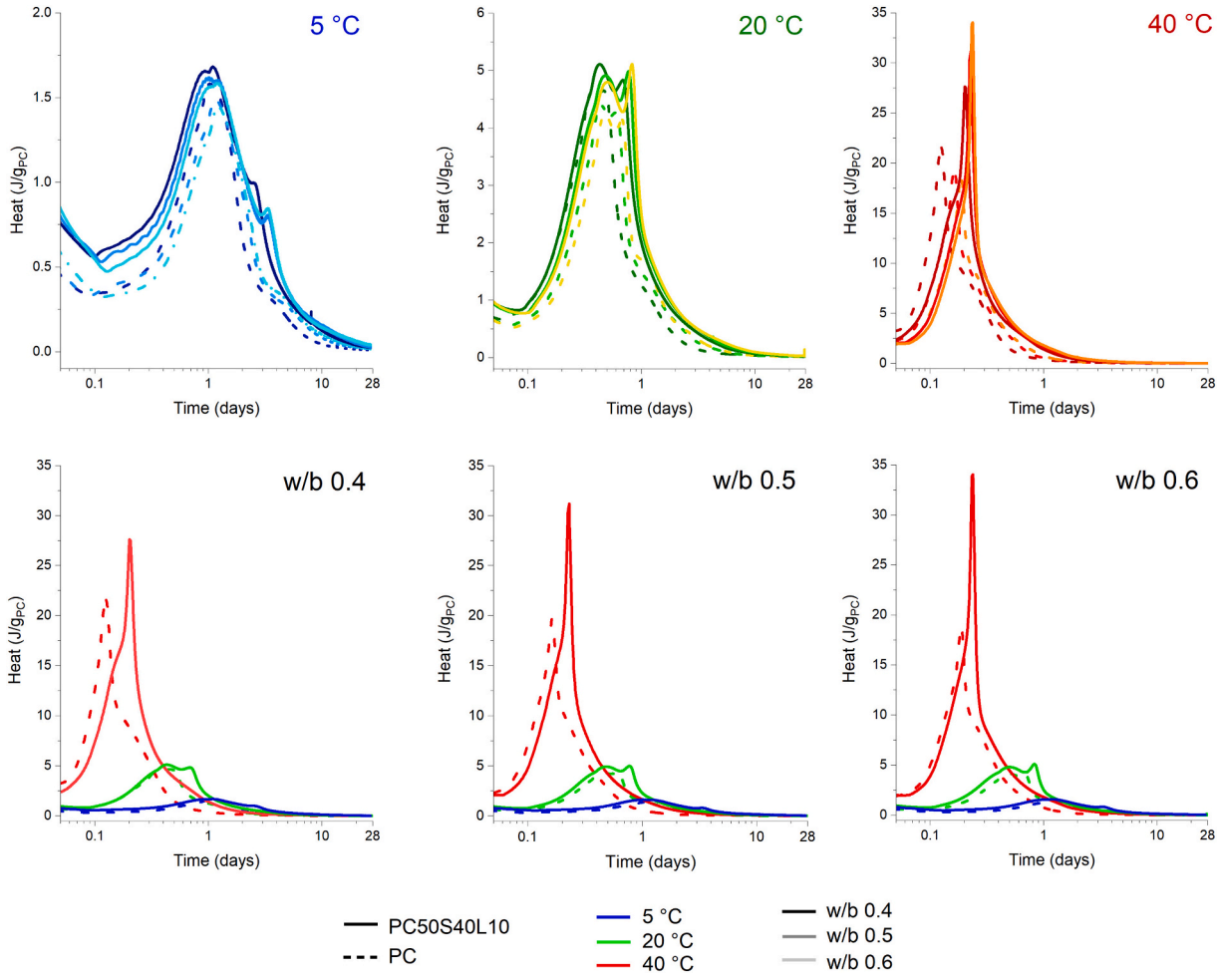

Fig. 4. Heat flow curves measured during isothermal hydration of ternary slag-limestone cement (PC50S40L10) and reference neat Portland cement (PC) for water/binder mass ratios (w/b) of 0.4, 0.5 and 0.6 cured at 5, 20 and 40 °C. Results are reported to the mass of Portland cement.

For each sample, 25 adjacent areas were mapped.

Image analysis targeted the segmentation of areas corresponding to residual unreacted slag. The cumulated area served as input in the calculation of the degree of reaction of slag over time. To this purpose, a custom-made image analysis routine was programmed in Python. The developed image analysis procedure consisted of a first step of equalizing the BSE image followed by grey level thresholding to separate hydrates from anhydrous slag and clinker phases. In a second step the slag and the clinker phases were distinguished using a k-means clustering algorithm based on the Mg, Si, Al, and Ca EDX elemental maps. An example of the segmentation of slag particles based on SEM-EDX mappings is given in Fig. 2.

To study the effect of w/b ratio and curing temperature on C-S-H composition, SEM-EDX point analyses of the binder matrix were measured on selected specimens cured for 28 days. EDX spectra of about 200 measurement points were collected for each studied specimen. A Zeiss EVO LS10 scanning electron microscope outfitted with a W-filament and operated at 15 kV acceleration voltage and working distance of 8.5 mm was used in combination with a Bruker XFlash 610-Mini detector to measure the EDX spectra. The element concentrations of Al, Si, Ca, Mg, Fe and S were calculated by the Bruker Esprit software based on a calibration against measured standards minerals (MAC Ltd.) and by correcting for matrix effects by the Phi-Rho-Z method. Cross-plotting of atomic (molar) elemental ratios with interpolation of tie lines was used to derive the C-S-H end-member composition as detailed in [51].

3. Results

3.1. Effect of w/b ratio and curing temperature on hydration heat

The cumulative hydration heat results of the pastes prepared at different water to binder ratios and cured at different temperatures are displayed in Fig. 3. The heat is shown normalized by the mass of PC in each sample. Reported in this way the blended cements invariably showed higher heat release than the Portland cements. This increase is attributed to a combination of the filler effect that enhances the hydration of the clinker phases at early ages and the hydration of the GGBFS at later ages. At a given temperature, the heat release was similar for all water to binder ratios at very early age, i.e. during the acceleration and maximum of the main clinker hydration event (Fig. 4). During the deceleration period and beyond a critical value, the cumulative heat curves started to diverge. Pastes of higher water to binder ratios reached higher cumulative heat values by 28 days, however this increase in heat did not scale linearly with the water to binder ratio, being larger between 0.4 and 0.5 than between 0.5 and 0.6. The effect of w/b ratio on hydration heat was similar for the blended and the reference cement. In contrast, curing temperature impacted the heat release of the blended and reference cements differently. For a constant w/b ratio an increase in curing temperature gave a much stronger increase in hydration heat for the blended cement than for the reference cement. For all water to binder ratios, the 40 °C cured blended cements invariably reached higher cumulative heat until 28 days than 20 and 5 °C cured blended cements. On the contrary, the hydration heat of the reference cements

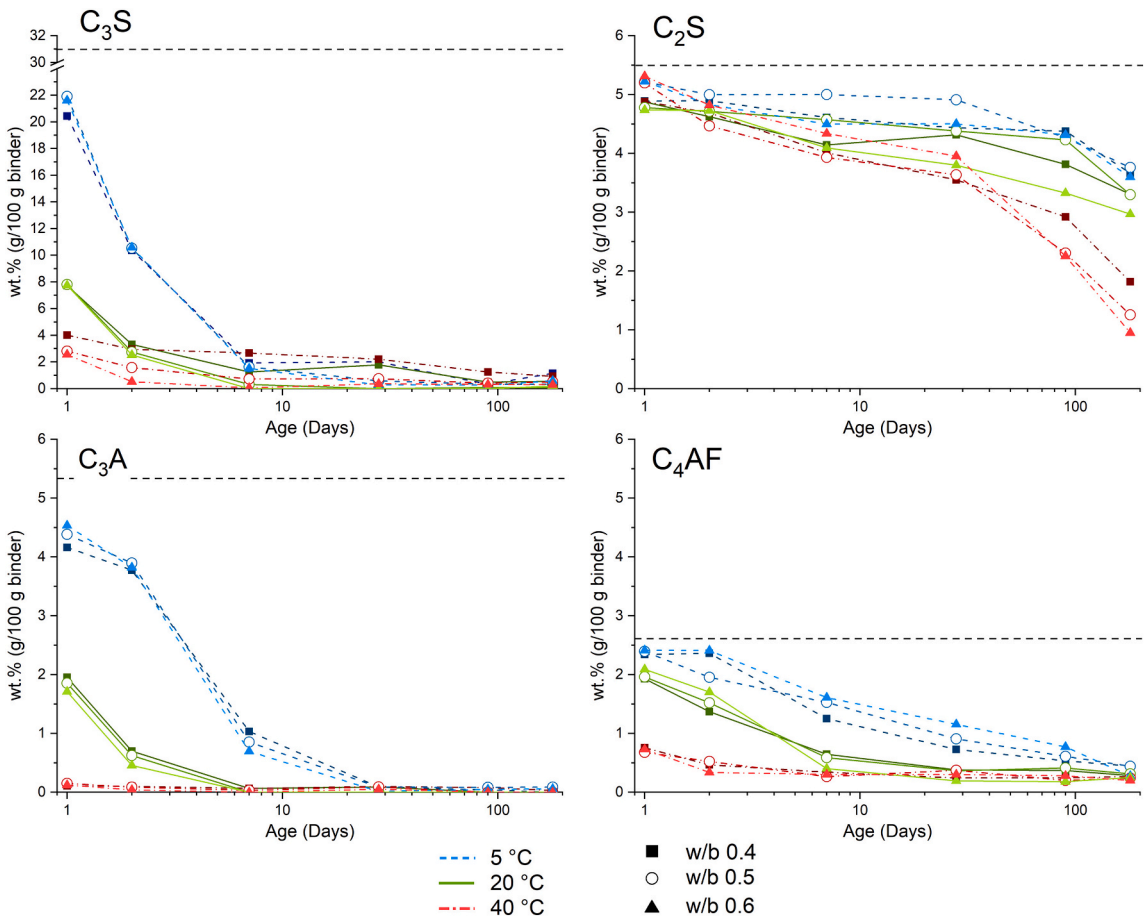

Fig. 5. Evolution of the individual clinker phase content during hydration of the ternary slag-limestone cement (PC50S40L10) for varying curing temperature and w/b ratio. The portrayed data were obtained by XRD-Rietveld analysis of hydration stopped cement powders. The horizontal dashed black line indicates the initial level of each clinker phase.

cured at different temperatures converged by 28 days. The effect of curing temperature on blended cements is well-known and explained by the higher apparent activation energy of pozzolanic reactions or slag hydration compared to clinker [20]. In addition, it is observed that the time gap between the main hydration peak and the sulfate depletion peak (the third peak in the heat flow curves in Fig. 4) shortens strongly with increase in temperature, almost coinciding with main hydration peak for curing at 40 °C. In addition, the sulfate depletion heat flow peak increases with curing temperature. The effect of water to binder ratio on the position and intensity of the sulfate depletion peak was less pronounced, however a minor delay and intensity increase is notable for higher water to binder ratios. The reference PC showed similar trends, however the sulfate depletion peak was much less pronounced.

3.2. *Effect of w/b ratio and curing temperature on constituent degree of reaction*

The hydration rates of individual constituents of the ternary slag-limestone cement were determined by Rietveld-XRD quantitative phase analysis and for slag also by BSE EDX IA. The evolution over time of the concentrations of the main clinker phases is shown in Fig. 5. Results are given for the various curing temperatures and w/b ratios included in this study. For clarity, only the result from the blended cements are displayed and discussed. The hydration rates of the clinker phases followed a well-known pattern. Alite and C_3A hydrated rapidly, i.e. within a few days at 20 and 40 °C, while ferrite (C_4AF) and in particular belite (β-C_2S) showed a slower rate of reaction. Belite was observed to experience a delay in the start of hydration compared to the other main clinker phases. Irrespective of the curing temperature or the w/b ratio, belite hydration was slow to insignificant over the first 28 days of curing. A delay in the hydration of belite in slag blended cements was observed before, and may arise from a competition with alite or slag hydration [25,26]. The effect of w/b ratio on the hydration of the clinker phases was found to be insignificant, in particular for the rapidly hydrating alite and C_3A phases. In contrast, the temperature of curing had a strong impact on the hydration rates of all clinker phases. The hydration rates of alite, C_3A and ferrite were strongly accelerated by increasing the curing temperature. However, after 180 days their reaction degrees converged. Belite hydration was accelerated as well by a rise in temperature, albeit after a prolonged period of slow reaction, which resulted in the observation that the reaction degrees of belite still show a difference depending on the curing temperature after 180 days.

The total clinker degree of reaction was calculated from the residual concentrations of the individual clinker phases at a given time compared to the initial concentrations ($t = 0$) of these phases. The evolution of the clinker degree of reaction until 180 days of hydration is given in Fig. 6a. Again, while the accelerating effect of the temperature increase on clinker hydration is clear, the effect of the w/b ratio is negligible at early age. Beyond 7 days of hydration the degree of reaction of the clinker is similar for all conditions. This implies that differences in cement properties (e.g. heat release) beyond 7 days are originating mainly from the other reactive constituents of the cement, i.e. the slag. The hydration of the slag is given as degree of reaction over time in Fig. 6b. The results shown in Fig. 6b were obtained by the PONKCS approach implemented in the XRD-Rietveld analysis to quantify the content of slag, which is a relatively new approach. The results were therefore cross-checked

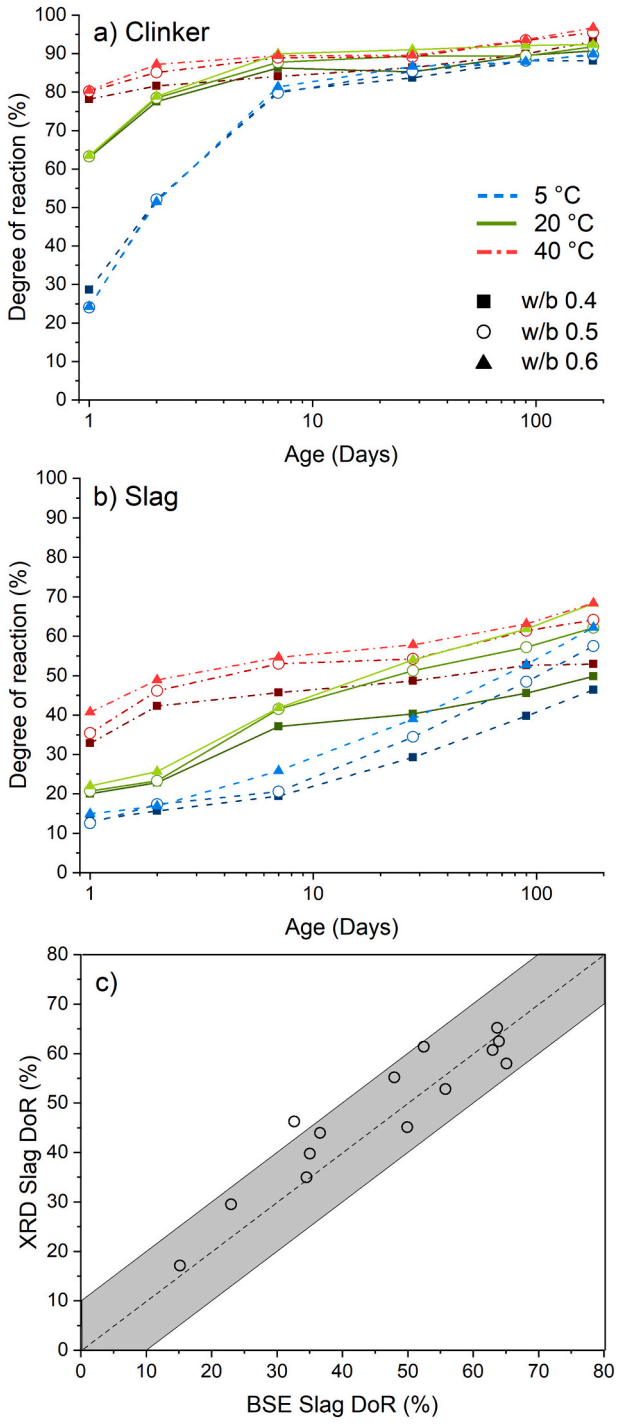

Fig. 6. Evolution over time of the degree of reaction of Portland clinker (a) and slag (b) during hydration of slag-limestone cement (PC50S40L10) at varying temperatures and w/b ratios. The portrayed data in a) and b) were obtained by XRD-Rietveld analysis of hydration stopped cement powders. c) Comparison between XRD and BSE image analysis results of slag degree of hydration (DoR), the grey area corresponds to a difference of 10% or less in measured values of slag degree of reaction.

against a more conventional analysis of BSE-EDX images on selected specimens covering all hydration ages, curing temperatures and w/b ratios. Both datasets are compared in Fig. 6c. The averaged absolute difference between the two measurement methods is 5% degree of reaction. With exception of 1 sample, all results were situated within a margin of error of 10% degree of reaction, being assumed as a general precision limit for SCM degree of reaction in blended cements [52,53]. Given the rather high uncertainty on the measurement, the slag degree of reaction data should still be interpreted with caution.

The effect of w/b ratio on slag degree of reaction was observed to be limited at early ages or low degrees of slag reaction. At later ages, i.e. from 3 to 7 days onwards depending on the curing temperature, the specimens prepared with a higher w/b ratio tend to reach higher degrees of slag reaction. Higher curing temperatures significantly accelerated slag reaction rates at early ages. At later ages hydration slowed down for the higher curing temperatures, the deceleration was stronger for samples prepared with a w/b ratio of 0.4 than samples prepared with higher w/b ratios (0.5, 0.6). By 180 days, the degree of reaction of the slag in the different systems tended to converge.

A quantitative assessment of the sensitivity of the hydration rate to the curing temperature was made by calculation of the apparent activation energy. Here, the apparent activation energy was calculated by fitting the degree of reaction to the exponential three-parameter equation as proposed by Poole et al. [54]. However, instead of using the degree of hydration based on calorimetry data of the cement as a whole, the degrees of reaction of each cement constituent from quantitative XRD/SEM analysis were fitted. This approach has two main advantages: 1) the apparent activation energies of the individual constituents can be estimated, and 2) the observed time span is extended up to 180 days instead of the 7 to 14 days of typical calorimetry measurements. The degree of reaction as a function of time, α (t), was fitted by Eq. (1):

$$\alpha(t) = \alpha_u exp^{-\left(\frac{\tau_c}{t+t_0}\right)^{\beta}} \quad (1)$$

where α_u is the ultimate degree of reaction (%), t is the curing age (days) and t_0 is a delay parameter (days). τ_c is the time parameter (days) for a given curing temperature, T_c, and β is an empirical parameter. For a given w/b ratio α_u and β were taken as constant in the fitting routine, t_0 was only allowed to vary from 0 in case of C_2S, which experienced a strong delay in hydration. The apparent activation energy, E_a, was calculated using the Arrhenius equation as:

$$E_a = -\frac{ln(\tau_c)}{(1/T_c)} \times R \quad (2)$$

where R is the universal gas constant (8.314 $J{\cdot}K^{-1}{\cdot}mol^{-1}$). Fig. 7 shows the fitting of the exponential equation to the constituent reaction degrees at 5, 20 and 40 °C. The data fitting of the 0.5 w/b ratio pastes are shown as example. It can be observed that the fitting curves generally correspond well with the measured data. Deviations of the measured data from the fitting curve are larger for cement constituents present in low concentrations (C_4AF, C_3A, C_2S). The scatter mainly originates from a magnification of the measurement uncertainty of the XRD-Rietveld results by the recalculation to degree of reaction. In case of slag, the scatter reflects the larger uncertainty in the XRD-PONKCS analysis (estimated at 10% in degree of reaction, see Fig. 6c).

The calculated apparent activation energies for w/b ratio 0.4, 0.5, and 0.6 are reported in Table 2. The reported apparent activation energies do not show a clear dependency on the w/b ratio. Both for the main clinker constituents, the slag and the clinker as a whole, the variations were minimal. The variations for C_4AF are higher, but it should be noted that for C_4AF the calculation is most affected by measurement data scatter as least abundant clinker constituent. The calculated apparent activation energies for alite of 32–34 kJ/mol are in line with earlier studies reporting values from 26 to 42 kJ/mol [55–58]. Also the values found for belite are within range of earlier reports, i.e. between 21 and 56 kJ/mol [57,59]. On the other hand, the calculated values for C_3A and C_4AF are higher than previously reported, i.e. 39–54 kJ/mol [56,57] and 34 kJ/mol [57], respectively. Previous studies considered the hydration of pure phases or their hydration in neat Portland cement. Therefore, the higher activation energies for C_3A and C_4AF may be due

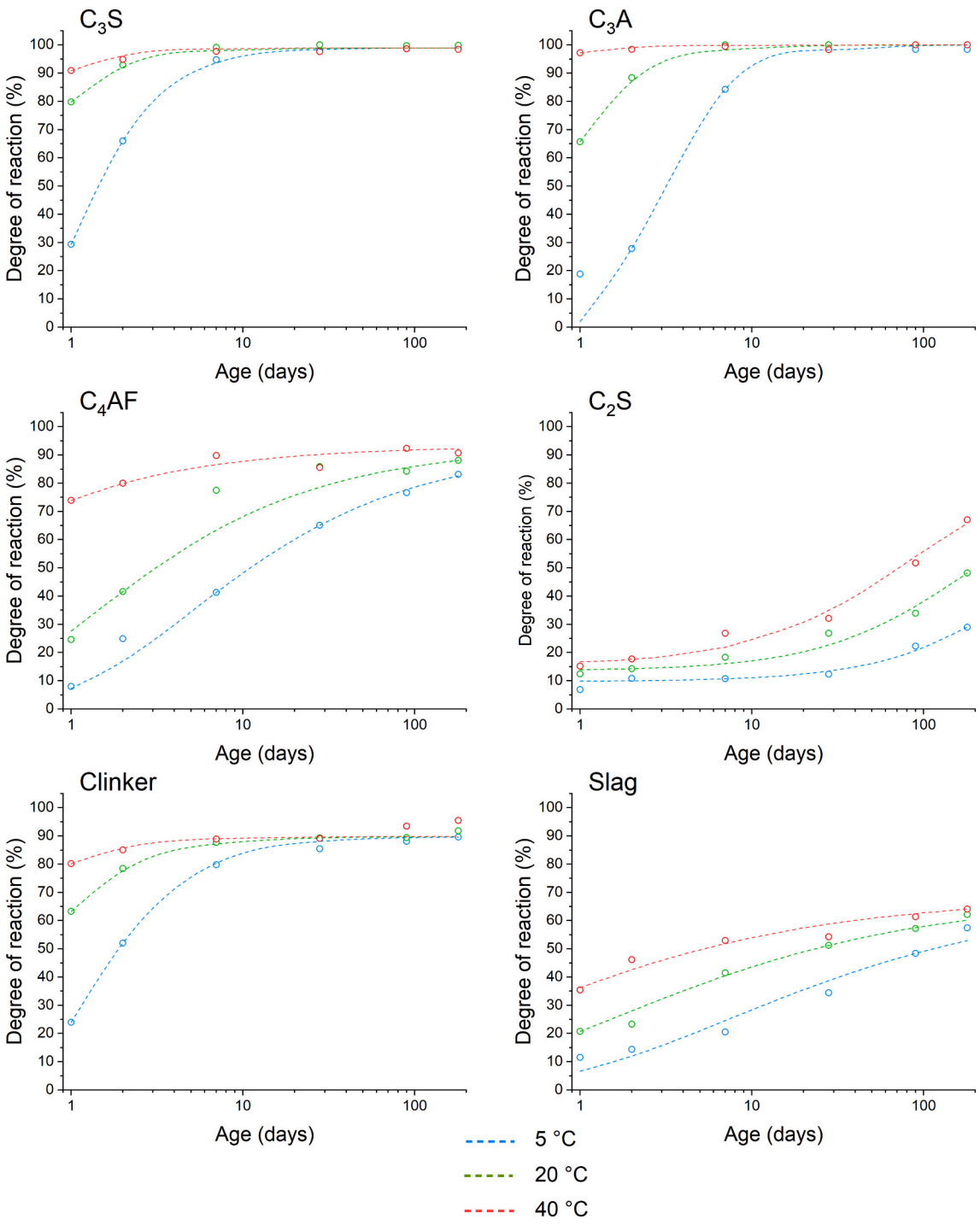

Fig. 7. Cement constituent degree of reaction for w/b 0.5 measured by XRD (open circles), fitted by the three-parameter exponential model (dashed lines).

to interactions with the cement additions, i.e. limestone, and slag, or to more rapid sulfate depletion. The clinker apparent activation energies, calculated as weighted average according to the mass proportion of each clinker constituent, correspond well to the values calculated from the curve fitting of the clinker degree of reaction data. This implies that, over the considered time period of 180 days, the temperature dependency of clinker hydration can be calculated from its phase composition. The slag apparent activation energies are within the range of previously reported literature values between 50 and 72 kJ/mol [17,20,21,60,61].

3.3. Effect of w/b ratio and curing temperature on hydration product formation

Fig. 8 shows the development of the bound water and the $Ca(OH)_2$ content over time of the PC50S40L10 samples prepared with the various w/b ratios and cured at different temperatures. The results reported in Fig. 8 were obtained by thermogravimetric analysis. The bound water content increases for all samples with time, as expected. A slightly higher ultimate bound water content is determined with increasing w/b ratios. The addition of more water provides more space to the system, which facilitates further reaction of slower reacting phases such as slag and belite (see Figs. 5 and 6).

Table 2
Calculated apparent activation energies for PC50S40L10 of the individual clinker constituents, the mass fraction weighted average of the individual clinker constituents, the clinker and slag. The calculations are based on the quantitative XRD results.

PC50S40L10			
w/b mass ratio	0.4	0.5	0.6
Apparent activation energy	(kJ/mol)	(kJ/mol)	(kJ/mol)
C_3S	32	34	34
C_2S	43	42	48
C_3A	63	63	62
C_4AF	63	85	72
Clinker phases weighted average	*39*	*41*	*41*
Clinker	40	40	39
Slag	67	63	63

Similar as described for the bound water content, more $Ca(OH)_2$ was present in the samples prepared with a higher w/b ratio. As QXRD results (see Fig. 6) show, there is hardly any difference in terms of clinker degree of reaction for higher w/b ratios, while instead for slag the degree of reaction is higher for higher w/b ratios. Therefore, the differences in the portlandite content may be explained by changes in the C-S-H stoichiometry for different w/b ratios. As is reported in the literature increasing the water to cement ratio lowers the Ca/Si in C-S-H and increases the $Ca(OH)_2$ phase content [62].

With increasing curing temperature, more water is bound in the samples, especially at early ages. At 40 °C, most of the water was bound within the first 7 days of hydration, while the sample cured at 5 °C reached a similar level only after 90 days of hydration. However, in contrast to what is typically found for Portland cement hydration, no "inversion effect" was observed in the case of the ternary slag-limestone cement up to 180 days in the current study. The "inversion effect" refers to the higher bound water levels and compressive strength obtained at later ages for low temperature cured cements compared to high temperature cured cements [63,64]. Instead, here, the bound water content of the samples cured at various temperatures converged to the same value only by 180 days.

The $Ca(OH)_2$ contents showed a slightly different development over time depending on the curing temperature. The $Ca(OH)_2$ content in the samples cured at 5 °C or 20 °C increased until 7 or 2 days respectively, before it slightly decreased again. At 40 °C, the $Ca(OH)_2$ content was already at its maximum value at 1 day and decreased over the entire measured time range (1–180 days). From 7 days on, the $Ca(OH)_2$ content was lowest in the sample cured at 40 °C, and highest in the sample cured at 5 °C. Both results indicate the enhancement of the reaction of the slag with increased curing temperatures, which leads to a higher and earlier decrease of $Ca(OH)_2$.

An insight of the effect of w/b ratio and curing temperature on the hydration product assemblage was obtained by XRD analysis. XRD scans in Fig. 9a illustrate the development of the hydration phase assemblage for the ternary slag limestone cement prepared at a w/b ratio of 0.5 and cured at 20 °C. At 1 day of hydration, ettringite and portlandite were identified as main crystalline hydration products. From 2 days of hydration onwards, hemicarboaluminate was present, while monocarboaluminate and hydrotalcite developed more slowly over time.

The effect of w/b ratio on the (crystalline) hydration products is shown in Fig. 9b. It can be observed that the w/b ratio does not change the hydrate assemblage qualitatively. The same products are formed, i.e. ettringite, hemicarboaluminate and monocarboaluminate hydrate as main calcium aluminate hydrates, hydrotalcite as Mg-Al hydrate mainly resulting from the hydration of slag, as well as portlandite as a hydration product of the calcium silicate clinker phases. Small differences were observed though. When overlaying the XRD patterns it is consistently seen that ettringite and hemicarboaluminate peak heights increase and become more crystalline (narrower) with increasing w/b ratio, also monocarboaluminate showed a similar trend. This trend was observed for all temperatures studied (not shown).

The effect of temperature is shown for 2 and 180 days of hydration in Fig. 9c for PC50S40L10 pastes prepared at a w/b ratio of 0.5. Overall, there was no major change in the hydration phase assemblage across the studied temperatures. At 2 days of hydration the effect of temperature on the hydrate assemblage is explained by the hydration kinetics of the clinker and slag phases. While at 5 °C only ettringite and portlandite can be observed, at 20 °C hemicarboaluminate is clearly present, and at 40 °C also weak peaks of hydrotalcite and monocarboaluminate are apparent. At 180 days all these phases have clearly formed for all temperatures. Comparing patterns at 180 days shows that ettringite and hemicarboaluminate peak intensities decrease with increasing temperature, conversely the monocarboaluminate and hydrotalcite peaks both increase with increasing temperature.

Quantification of the hydration products by XRD-Rietveld refinement confirmed the qualitative trends described above for the calcium aluminium hydrates and $Ca(OH)_2$. Fig. 10 shows that the portlandite contents for samples cured at 20 °C and 40 °C are more or less constant from 2 until 180 days, although slightly lower in value for 40 °C. At 5 °C, the portlandite content is initially lower because of the slower hydration

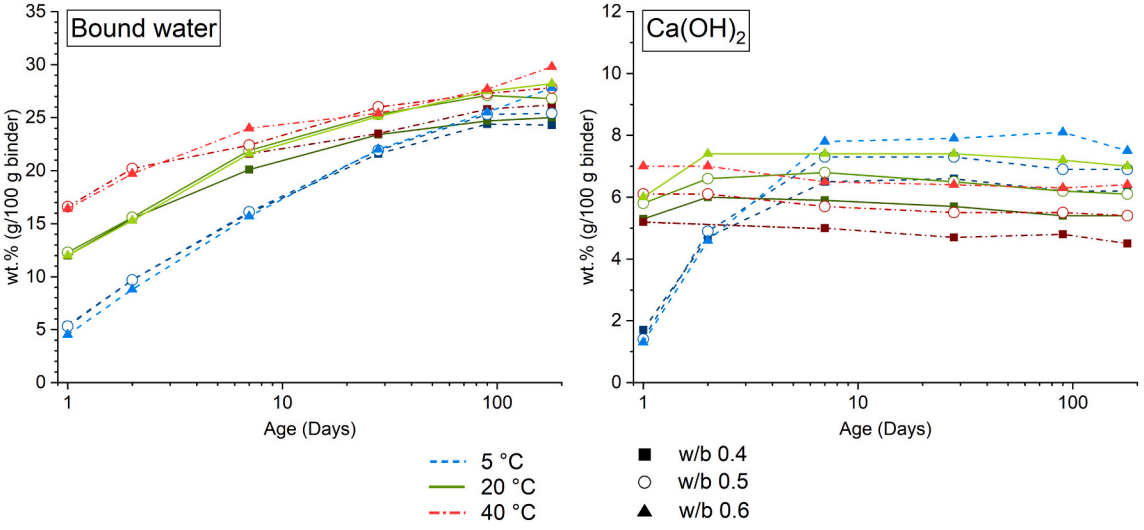

Fig. 8. Time evolution of bound water and $Ca(OH)_2$ content in hydrating PC50S40L10 prepared at 0.4, 0.5 and 0.6 w/b ratio, and cured at 5, 20 and 40 °C. The plotted data are calculated from TGA measurements on hydration stopped pastes.

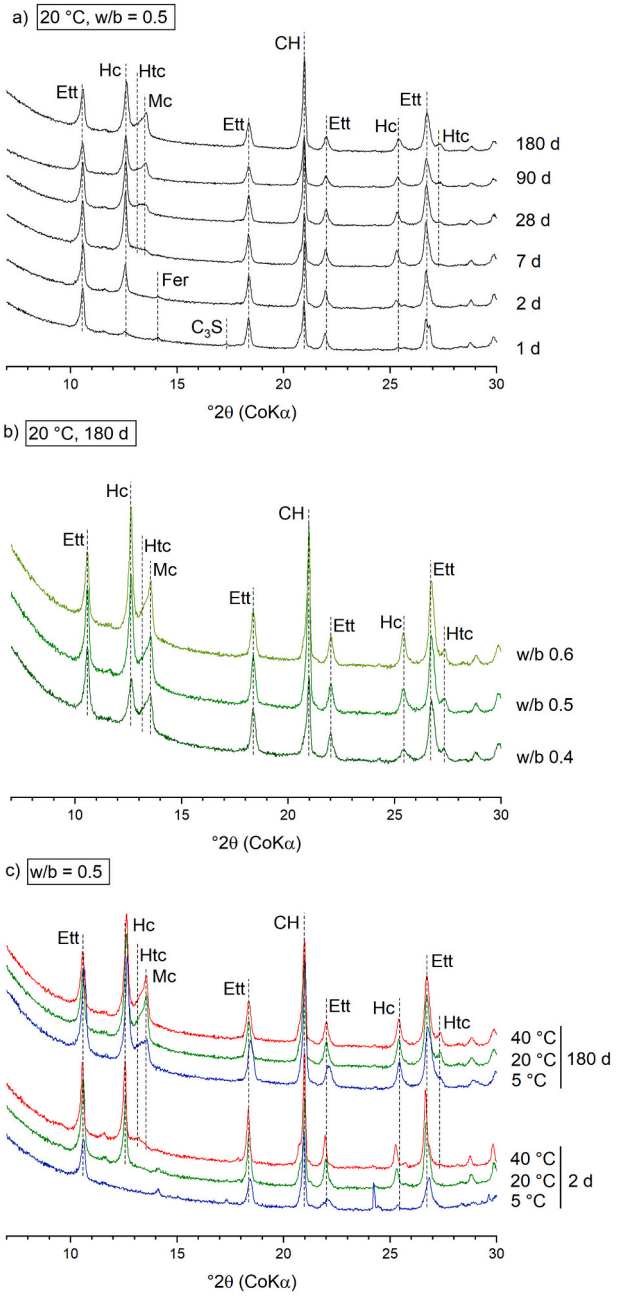

Fig. 9. XRD scans of PC50S40L10 fresh specimens of: a) a hydration time-series from 1 to 180 days for a curing temperature of 20 °C and w/b ratio of 0.5; b) a w/b ratio series of 0.4, 0.5 and 0.6 cured at 20 °C for 180 days; c) a curing temperature series of 5, 20 and 40 °C at 2 and 180 days of hydration and w/b ratio of 0.5. The XRD reflection peaks of the main hydration products are marked as follows: Ett stands for ettringite, Hc for hemicarboaluminate, Htc for hydrotalcite, Mc for monocarboaluminate, CH for portlandite, Fer for C_4AF, and C_3S for alite.

of alite, but eventually ends up slightly higher in value than at 20 and 40 °C. The portlandite content increases with increasing water to binder ratio thereby following the same trend as the TGA results.

Ettringite formation on the other hand is clearly affected by both temperature and water to binder ratio. The ettringite contents decrease with increasing curing temperature, the difference between 5 °C and 40 °C amounts to about 5 wt% after 180 days of hydration. Overall, ettringite levels were found to be stable after its maximum value has been reached. Increased w/b ratios correlated with higher ettringite contents, the difference among w/b ratios was established even early on during the hydration.

Carboaluminate hydrates developed upon depletion of the sulfate carriers and further hydration of C_3A and C_4AF. First hemicarboaluminate was formed, followed by monocarboaluminate as shown by the quantification results in Fig. 10. Hemicarboaluminate contents reached lower levels at 40 °C, while at 20 and 5 °C similar amounts were found. After reaching a maximum, hemicarboaluminate decreased slightly over time for all temperatures. For 5 and 20 °C the maximum hemicarboaluminate content varied with the water to binder ratio. The higher the water to binder ratio, the higher the maximum level. Monocarboaluminate developed more slowly.

Hydrotalcite formation correlated with the hydration rate of the slag. After an initial gain to about 4–5 wt%, the formation of hydrotalcite was more gradual. In case of hydrotalcite, temperature gain had no adverse effect on the final achievable content, indicating the stability of this phase. There was no noticeable effect of water to binder ratio.

The composition of the main hydrate phase, C-S-H, is estimated by analyzing point clouds of elemental ratios measured by SEM-EDX point analyses. The measured points were manually selected and situated within the cement matrix, i.e. the hydrate binder phase. Fig. 11 shows Al/Ca versus Si/Ca cross-plots for selected w/b ratios and curing temperatures that represent the extremes and center point of the experimental design to provide insight on the extent of variation of the C-S-H composition. All analyses were carried out on specimens that were cured for 28 days. Due to the very fine texture and intermixing of the cement hydrates, most points include contributions from various hydrates, resulting in averaged elemental ratios falling along mixing lines between the main hydrates, i.e. C-S-H, AFm/ettringite, and portlandite. Fig. 11 shows that most point analyses were distributed along the mixing line between AFm and ettringite phases on one end (Si/Ca of 0 and Al/Ca ratio of 0.5 and 0.33, respectively) and C-S-H on the other end. The mixing line between portlandite (situated at the origin of the plot) and C-S-H was less populated by point analyses, yet easily positioned at the lower edge of the data point cloud. The C-S-H composition was then estimated from the coordinates of the intersection point of the two mixing lines [51]. A comparison of the point clouds and the constructed mixing lines in Fig. 11 showed that the intersection points shifted to higher Si/Ca for increasing curing temperature (cf. Fig. 11b) and increasing w/b ratio (cf. Fig. 11c). This translated in lower C-S-H Ca/Si ratios for higher curing temperatures and higher water to binder ratios. Differences in C-S-H Al/Ca were less pronounced but followed a similar trend. Values for both C-S-H Si/Ca and Al/Ca are provided in Table 3.

4. Discussion

The results show the impact of water to binder ratio and curing temperature on cement hydration kinetics and hydrate assemblage of ternary slag-limestone blended cement pastes. The water to binder ratio mainly affects the available water and space for hydrates to grow, while the curing temperature directly affects reaction kinetics of the cement components and the solubilities of the hydrates. The quantification of consumption and formation of individual phases revealed differential phase-specific responses to changes in w/b ratio and temperature.

4.1. Hydration kinetics

The early age (until 1 day) hydration kinetics were strongly accelerated by temperature increase, while the water to binder ratio had only a limited impact as sufficient water and space was available for hydration at that time. Alite reacted rapidly and was practically completely hydrated by 7 days at 20 °C (Fig. 5). This is faster than usually reported for neat Portland cement [63,65,66] and is explained by the high initial fineness of the clinker, the relatively high clinker replacement rate and the enhanced filler effect by the limestone constituent [35]. The temperature dependency of the alite hydration rate was observed to be similar to neat Portland cement [58]. In line with earlier findings, the

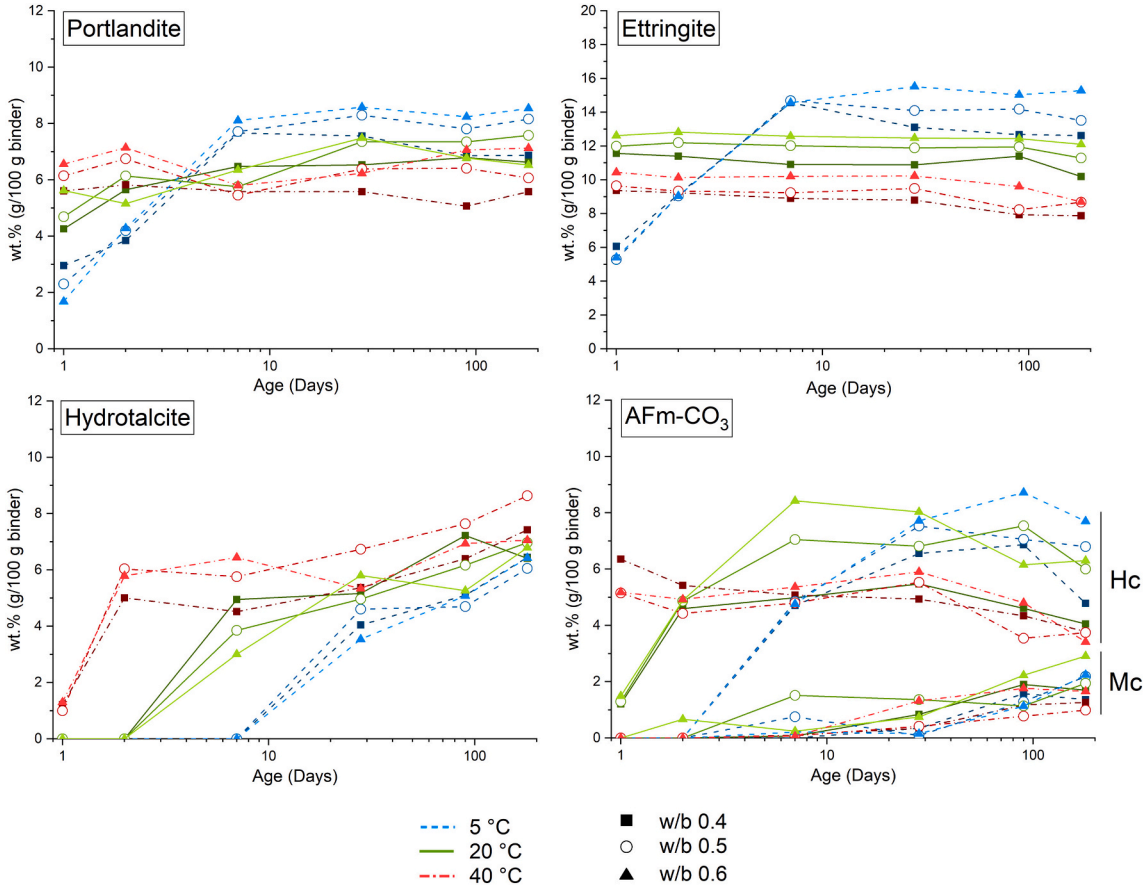

Fig. 10. XRD-Rietveld quantification results showing the formation of portlandite, ettringite, hydrotalcite and AFm-CO_3 (hemi- and monocarboaluminate; Hc and Mc, resp.) over time for pastes prepared at w/b ratios of 0.4, 0.5 and 0.6, and cured at 5, 20 and 40 °C.

main reaction of C_3A occurred rapidly at early age after sulfate depletion [67,68]. Compared to alite, the C_3A hydration rate was accelerated to a greater extent by increasing temperature (Fig. 5). Moreover, the C_3A apparent activation energy was calculated to be higher than reported in earlier studies on neat Portland cement [56,57]. This correlated with a higher and earlier sulfate depletion heat flow peak observed by calorimetry for the slag-limestone cement. Higher water to binder ratios increased the sulfate depletion peak height, therefore the higher reaction rate of C_3A in the slag-limestone cement can be partially related to the availability of more space and water. For both higher temperature and higher w/b ratio, the earlier occurrence of the sulfate depletion peak could be related to the accelerated clinker and slag hydration leading to more rapid consumption of sulfate in solution by precipitation of ettringite and sorption on C-S-H from slag hydration [25,69]. As both C_3A and slag have higher apparent activation energies than alite, the optimization of the cement sulfate dosage should take into account the anticipated curing or ambient temperature to avoid undersulfation and suboptimal cement performance [38].

Slag was found to react significantly (10–40%) already after 1 day (Fig. 6b), in line with a number of previous studies [12,13,25,53,70]. Other studies have reported lower degrees of slag reaction (<10%) at 3 days or even earlier [12,19,71]. The discrepancy in the literature is partly explained by differences in material properties and curing conditions, but also by differences in the measurement methodologies. On the one hand slag and cement composition and fineness, clinker replacement rate, water to binder ratio and curing temperature are all known to affect slag reactivity [11,12,19]. Here both the clinker and the slag were milled relatively finely, while the slag content was not too high, all these give positive feedback on slag reactivity. On the other hand, measurement techniques such as scanning electron microscopy and XRD-PONKCS tend to report high degrees of reaction at early ages because of difficulties in recognizing small particles, or measurement uncertainty, respectively. In contrast, measurements of slag reaction degree by selective dissolution tend to be underestimated [12,53].

At later age, the cement constituent reaction degrees tend to converge for the different curing temperatures. However, full convergence could not be reached by 180 days of hydration, indicating a remaining positive effect of higher temperature curing even at later hydration times. This was in particular the case for slow reacting phases such as slag. It is not immediately clear why elevated temperature curing has a long-lasting positive effect on slow reacting phases. Possibly, this is related to differences in the cement microstructure occurring in case of quasi-simultaneous (e.g. 40 °C) vs. sequential (5 °C) hydration of clinker and slag [72]. Provision of more space, by increasing the water to binder ratio, mainly impacted the degree of reaction of slower reacting phases such as slag, and to a lesser extent, belite. For slag, the difference was significant when increasing the w/b ratio from 0.4 to 0.5. Differences between 0.5 and 0.6 w/b ratio were smaller and mostly insignificant for direct measurements of slag reaction degree. These findings are generally in line with previous studies on the effect of water to binder ratio on the hydration of slag blended cements [11,19]. Generally, however, the increase in slag degree of reaction by using higher w/b ratio did not compensate for the increase in the volume of pore space to be filled. The initial slow reaction of belite remains a point of discussion. Earlier research indicated that belite hydration could be retarded by a high solution supersaturation caused by the dissolution of other calcium silicates such as alite [73]. This however does not explain the even longer retardation in combination with slag.

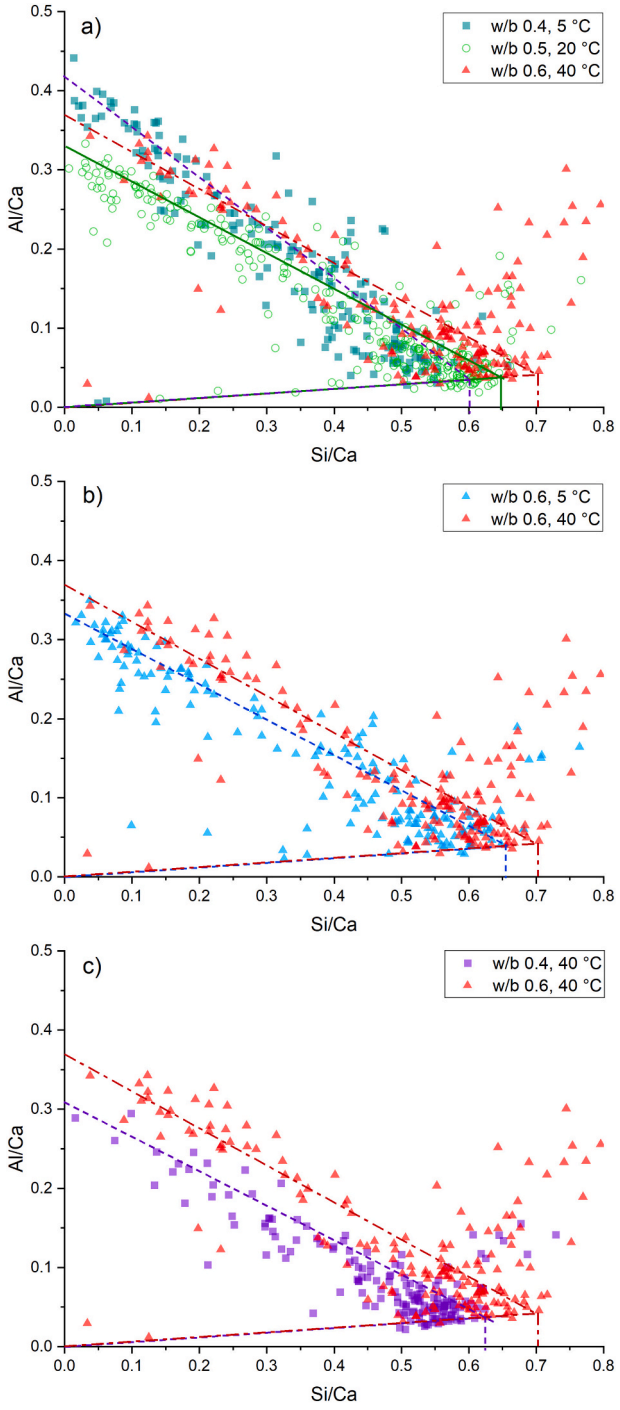

Fig. 11. C-S-H chemical composition from cross-plots of Al/Ca versus Si/Ca ratios of individual SEM-EDX point analyses of the ternary cements cured for 28 days comparing a) simultaneously increasing w/b ratio and curing temperature (extremes and center point of experimental design), b) different curing temperatures for a given w/b ratio of 0.6, c) different water to binder ratios for a given curing temperature of 40 °C.

4.2. Hydration products

The water to binder ratio and curing temperature were observed not to change the type of hydration products formed, but significantly changed the proportions of the major hydration products (Fig. 10). Ettringite and portlandite contents experienced a temperature cross-over effect with lower curing temperature phase contents eventually overtaking higher curing temperature phase contents at later ages

Table 3
C-S-H composition elemental ratio determined by SEM-EDX point analyses on 28 days cured specimens for selected combinations of w/b ratio and curing temperatures.

w/b mass ratio (–)	Curing temperature (°C)	Si/Ca	Al/Ca
0.4	5	0.60 ± 0.02	0.035 ± 0.01
0.4	40	0.62 ± 0.02	0.038 ± 0.01
0.5	20	0.65 ± 0.02	0.039 ± 0.01
0.6	5	0.66 ± 0.02	0.040 ± 0.01
0.6	40	0.70 ± 0.02	0.042 ± 0.01

(Fig. 10). The difference between slag and clinker hydration rates is larger at low temperatures, and a slow slag hydration enables to reach higher portlandite and ettringite levels in the system. At higher temperatures, a substantial part of the $Ca(OH)_2$ released by clinker hydration is immediately consumed by the slag reaction. In consequence, the curing temperature changes the cement hydrate assemblage by accelerating the hydration rates of the clinker and slag to different extents. However, the convergence of bound water contents and, to some extent, slag degree of reaction at later age could be expected to result in a convergence of hydrate assemblages as well. This trend is observed neither in the XRD nor in the TGA results. This discrepancy is explained by variations in C-S-H composition, i.e. reduced C-S-H water content at higher curing temperatures [74,75] and lower Ca/Si ratios of C-S-H with increasing w/b ratios and increasing curing temperature (Fig. 11) [62]. The observed decrease in ettringite content with increasing temperature correlates with increasing ettringite solubility with increasing temperature [63,65,76], and in turn with higher sulfate sorption or uptake in C-S-H at higher temperatures [77,78]. Consequently, at 40 °C Al and S are expected to be taken up more by the C-S-H [79,80] rather than to precipitate as ettringite.

In line with previous studies, kinetics also affect the formation of AFm and hydrotalcite hydration products. Hemicarboaluminate is well known to form initially during cement hydration, while monocarboaluminate is thermodynamically more stable but develops later [30]. Hydrotalcite is formed during hydration of slag, however by XRD the appearance of hydrotalcite is only detected at relatively late hydration ages. This indicates that hydrotalcite at (very) early ages is lacking long-range order and crystallizes over time. This behavior is quite typical for crystalline cement hydration products [81,82]. Besides hydrotalcite, also ettringite and AFm are shown to increase in crystallinity over time and with increasing w/b ratio (see Fig. 9). Precipitation of more disordered phases at the initial stages offers kinetically favorable pathways to rapidly reduce solution supersaturation, the subsequent increase of crystallinity can be explained by the thermodynamically controlled Ostwald ripening phenomenon. The higher crystallinities obtained for higher w/b ratio would as such be explained by the availability of more water and pore space enabling the system to evolve further towards thermodynamic equilibrium.

5. Conclusions

The impact of water to binder ratio (0.4, 0.5, 0.6) and curing temperature (5, 20, 40 °C) on the hydration kinetics of ternary slag-limestone blended cement pastes was studied quantitatively using a combination of isothermal calorimetry, TGA, XRD and SEM techniques. The degree of reaction of the individual cement components was measured and their dependence on water to binder ratio and curing temperature was established.

The variation in the water to binder ratios studied did not significantly impact the early age hydration kinetics. However, at later ages cements prepared at higher water to binder ratios reached higher degrees of reaction for slower reacting slag and clinker phases like belite. The water to binder ratio had a minor impact on the type and contents of hydration products formed. It is notable that hydration products reached

a higher crystallinity in pastes prepared at higher water to binder ratio.

In contrast, the results clearly show early age acceleration of the hydration kinetics by increasing the curing temperature from 5 to 40 °C. The hydration of alite was the least sensitive to a change in temperature due to its lowest apparent activation energy of all cement phases. C_3A, C_4AF and slag showed significantly higher activation energies, and their hydration is consequently accelerated to a greater extent by a rise in curing temperature. This phase specific effect of temperature can cause modifications to the sequence of hydration reactions and lead to sub-optimal performance, for instance by causing the sulfate depletion event to occur before the main alite hydration peak. Curing at 40 °C increased the reaction of slag considerably at early age and had an enduring positive effect on slag degree of reaction. No late age cross-over by lower curing temperatures was observed until 180 days of hydration. Curing at higher temperature resulted in lower portlandite and ettringite contents. This is partially caused by the enhanced reaction rate and degree of the slag but is also tentatively related to a change in C-S-H stoichiometry.

CRediT authorship contribution statement

Ruben Snellings: Methodology, Investigation, Formal analysis, Visualization, Writing – Original draft preparation, Supervision. **Alisa Machner**: Methodology, Investigation, Writing – Review & editing. **Gerd Bolte**: Conceptualization, Investigation, Resources. **Hadi Kamyab**: Methodology, Validation, Investigation. **Pawel Durdzinski**: Methodology, Resources, Writing – Review & editing. **Priscilla Teck**: Methodology, Software, Investigation. **Maciej Zajac**: Conceptualization, Validation, Writing – Review & editing. **Arnaud Muller**: Conceptualization, Writing – Review & editing, Project administration. **Klaartje De Weerdt**: Writing – Review & editing, Supervision. **Mohsen Ben Haha**: Conceptualization, Writing – Review & editing, Supervision, Funding acquisition.

Declaration of competing interest

The authors declare that they have no known competing financial interests or personal relationships that could have appeared to influence the work reported in this paper.

Acknowledgements

Willem Stuyck, Myrjam Mertens, Bo Peeraer, Sten Janssen and Raymond Kemps are gratefully acknowledged for the diligent preparation and analytical measurements of the paste samples. We would also like to thank Tone H. Nilsen, Andreas Markali, Oda Tjetland and Caroline K. Hallerud for their help in sample preparation and analysis at NTNU.

Funding

This work was supported by the European Union's Horizon 2020 - Research and Innovation Framework Programme under grant agreement No 760639.

References

[1] G. Osborne, Durability of Portland blast-furnace slag cement concrete, Cem. Concr. Compos. 21 (1999) 11–21.
[2] J. Bijen, Benefits of slag and fly ash, Constr. Build. Mater. 10 (1996) 309–314.
[3] W. Matthes, A. Vollpracht, Y. Villagrán, S. Kamali-Bernard, D. Hooton, E. Gruyaert, M. Soutsos, N.De Belie, Ground granulated blast-furnace slag, in: Properties of Fresh and Hardened Concrete Containing Supplementary Cementitious Materials, Springer, 2018, pp. 1–53.
[4] M.C. Juenger, R. Snellings, S.A. Bernal, Supplementary cementitious materials: new sources, characterization, and performance insights, Cem. Concr. Res. 122 (2019) 257–273.
[5] C. Shi, B. Qu, J.L. Provis, Recent progress in low-carbon binders, Cem. Concr. Res. 122 (2019) 227–250.
[6] M.B. Haha, F. Winnefeld, A. Pisch, Advances in understanding ye'elimite-rich cements, Cem. Concr. Res. 123 (2019), 105778.
[7] G. Bolte, M. Zajac, J. Skocek, M.B. Haha, Development of composite cements characterized by low environmental footprint, J. Clean. Prod. 226 (2019) 503–514.
[8] J. Skibsted, R. Snellings, Reactivity of supplementary cementitious materials (SCMs) in cement blends, Cem. Concr. Res. 124 (2019), 105799.
[9] M.B. Haha, B. Lothenbach, G. Le Saout, F. Winnefeld, Influence of slag chemistry on the hydration of alkali-activated blast-furnace slag — part II: effect of Al2O3, Cem. Concr. Res. 42 (2012) 74–83.
[10] M.B. Haha, B. Lothenbach, G. Le Saout, F. Winnefeld, Influence of slag chemistry on the hydration of alkali-activated blast-furnace slag — part I: effect of MgO, Cem. Concr. Res. 41 (2011) 955–963.
[11] J. Lumley, R. Gollop, G. Moir, H. Taylor, Degrees of reaction of the slag in some blends with Portland cements, Cem. Concr. Res. 26 (1996) 139–151.
[12] V. Kocaba, E. Gallucci, K.L. Scrivener, Methods for determination of degree of reaction of slag in blended cement pastes, Cem. Concr. Res. 42 (2012) 511–525.
[13] R. Snellings, T. Paulhiac, K. Scrivener, The effect of mg on slag reactivity in blended cements, Waste Biomass Valoriz. 5 (2014) 369–383.
[14] E. Lang, Blast furnace cements, in: J. Bensted, P. Barnes (Eds.), Structure and performance of cements, Taylor & Francis, 2002, pp. 310–325.
[15] M. Moranville-Regourd, S. Kamali-Bernard, Cements made from blastfurnace slag, in: P. Hewlett, M. Liska (Eds.), Lea's Chemistry of Cement and Concrete, Butterworth-Heinemann, London, 2019, pp. 469–508.
[16] K.C. Reddy, K.V. Subramaniam, Quantitative phase analysis of slag hydrating in an alkaline environment, J. Appl. Crystallogr. 53 (2020).
[17] Z. Sun, A. Vollpracht, Isothermal calorimetry and in-situ XRD study of the NaOH activated fly ash, metakaolin and slag, Cem. Concr. Res. 103 (2018) 110–122.
[18] R. Snellings, Surface chemistry of calcium aluminosilicate glasses, J. Am. Ceram. Soc. 98 (2015) 303–314.
[19] J. Escalante, L. Gomez, K. Johal, G. Mendoza, H. Mancha, J. Mendez, Reactivity of blast-furnace slag in Portland cement blends hydrated under different conditions, Cem. Concr. Res. 31 (2001) 1403–1409.
[20] C. Castellano, V. Bonavetti, H. Donza, E. Irassar, The effect of w/b and temperature on the hydration and strength of blastfurnace slag cements, Constr. Build. Mater. 111 (2016) 679–688.
[21] S. Barnett, M. Soutsos, S. Millard, J. Bungey, Strength development of mortars containing ground granulated blast-furnace slag: effect of curing temperature and determination of apparent activation energies, Cem. Concr. Res. 36 (2006) 434–440.
[22] <Escalante-Garcia&Sharp2001.pdf>.
[23] M. Moesgaard, S.L. Poulsen, D. Herfort, M. Steenberg, L.F. Kirkegaard, J. Skibsted, Y. Yue, G. Scherer, Hydration of blended Portland cements containing calcium-aluminosilicate glass powder and limestone, J. Am. Ceram. Soc. 95 (2012) 403–409.
[24] R. Taylor, I.G. Richardson, R.M.D. Brydson, Composition and microstructure of 20-year-old ordinary Portland cement–ground granulated blast-furnace slag blends containing 0 to 100% slag, Cem. Concr. Res. 40 (2010) 971–983.
[25] S. Adu-Amankwah, M. Zajac, C. Stabler, B. Lothenbach, L. Black, Influence of limestone on the hydration of ternary slag cements, Cem. Concr. Res. 100 (2017) 96–109.
[26] M. Whittaker, M. Zajac, M. Ben Haha, F. Bullerjahn, L. Black, The role of the alumina content of slag, plus the presence of additional sulfate on the hydration and microstructure of Portland cement-slag blends, Cem. Concr. Res. 66 (2014) 91–101.
[27] E. Berodier, K. Scrivener, Evolution of pore structure in blended systems, Cem. Concr. Res. 73 (2015) 25–35.
[28] K. De Weerdt, M.B. Haha, G. Le Saout, K.O. Kjellsen, H. Justnes, B. Lothenbach, Hydration mechanisms of ternary Portland cements containing limestone powder and fly ash, Cem. Concr. Res. 41 (2011) 279–291.
[29] M. Antoni, J. Rossen, F. Martirena, K. Scrivener, Cement substitution by a combination of metakaolin and limestone, Cem. Concr. Res. 42 (2012) 1579–1589.
[30] B. Lothenbach, G. Le Saout, E. Gallucci, K. Scrivener, Influence of limestone on the hydration of Portland cements, Cem. Concr. Res. 38 (2008) 848–860.
[31] T. Matschei, B. Lothenbach, F.P. Glasser, The role of calcium carbonate in cement hydration, Cem. Concr. Res. 37 (2007) 551–558.
[32] A.M. Ramezanianpour, R.D. Hooton, A study on hydration, compressive strength, and porosity of Portland-limestone cement mixes containing SCMs, Cem. Concr. Compos. 51 (2014) 1–13.
[33] A. Schöler, B. Lothenbach, F. Winnefeld, M. Zajac, Hydration of quaternary Portland cement blends containing blast-furnace slag, siliceous fly ash and limestone powder, Cem. Concr. Compos. 55 (2015) 374–382.
[34] R. Snellings, Solution-controlled dissolution of supplementary cementitious material glasses at pH 13: the effect of solution composition on glass dissolution rates, J. Am. Ceram. Soc. 96 (2013) 2467–2475.
[35] E. Berodier, K. Scrivener, Understanding the filler effect on the nucleation and growth of C-S-H, J. Am. Ceram. Soc. 97 (2014) 3764–3773.
[36] L. Courard, D. Herfort, Y. Villagrán, Limestone powder, in: Properties of Fresh and Hardened Concrete Containing Supplementary Cementitious Materials, Springer, 2018, pp. 123–151.
[37] A. Kumar, T. Oey, G.P. Falla, R. Henkensiefken, N. Neithalath, G. Sant, A comparison of intergrinding and blending limestone on reaction and strength evolution in cementitious materials, Constr. Build. Mater. 43 (2013) 428–435.
[38] S. Adu-Amankwah, L. Black, J. Skocek, M.B. Haha, M. Zajac, Effect of sulfate additions on hydration and performance of ternary slag-limestone composite cements, Constr. Build. Mater. 164 (2018) 451–462.

[39] B. Kolani, L. Buffo-Lacarrière, A. Sellier, G. Escadeillas, L. Boutillon, L. Linger, Hydration of slag-blended cements, Cem. Concr. Compos. 34 (2012) 1009–1018.
[40] J. Skocek, M. Zajac, C. Stabler, M.B. Haha, Predictive modelling of hydration and mechanical performance of low ca composite cements: possibilities and limitations from industrial perspective, Cem. Concr. Res. 100 (2017) 68–83.
[41] G. De Schutter, Hydration and temperature development of concrete made with blast-furnace slag cement, Cem. Concr. Res. 29 (1999) 143–149.
[42] A.K. Schindler, K.J. Folliard, Heat of hydration models for cementitious materials, ACI Mater. J. 102 (2005) 24.
[43] R. Snellings, J. Chwast, Ö. Cizer, N. De Belie, Y. Dhandapani, P. Durdzinski, J. Elsen, J. Haufe, D. Hooton, C. Patapy, RILEM TC-238 SCM recommendation on hydration stoppage by solvent exchange for the study of hydrate assemblages, Mater. Struct. 51 (2018) 172.
[44] B. Lothenbach, P. Durdzinski, K. De Weerdt, Thermogravimetric analysis, in: K. L. Scrivener, R. Snellings, B. Lothenbach (Eds.), A Practical Guide to Microstructural Analysis of Cementitious Materials, CRC Press, Boca Raton, 2016, pp. 179–213.
[45] R. Snellings, X-ray powder diffraction applied to cement, in: K.L. Scrivener, R. Snellings, B. Lothenbach (Eds.), A Practical Guide to Microstructural Analysis of Cementitious Materials, CRC Press, Boca Raton, 2016, pp. 107–176.
[46] D. Jansen, F. Goetz-Neunhoeffer, C. Stabler, J. Neubauer, A remastered external standard method applied to the quantification of early OPC hydration, Cem. Concr. Res. 41 (2011) 602–608.
[47] B.H. O'Connor, M.D. Raven, Application of the rietveld refinement procedure in assaying powdered mixtures, Powder Diffract. 3 (1988) 2–6.
[48] E.E. Chang, C.H. Chen, Y.H. Chen, S.Y. Pan, P.C. Chiang, Performance evaluation for carbonation of steel-making slags in a slurry reactor, J. Hazard. Mater. 186 (2011) 558–564.
[49] N.V.Y. Scarlett, I.C. Madsen, Quantification of phases with partial or no known crystal structures, Powder Diffract. 21 (2006) 278–284.
[50] R. Snellings, A. Salze, K. Scrivener, Use of X-ray diffraction to quantify amorphous supplementary cementitious materials in anhydrous and hydrated blended cements, Cem. Concr. Res. 64 (2014) 89–98.
[51] K. Scrivener, R. Snellings, B. Lothenbach, A Practical Guide to Microstructural Analysis of Cementitious Materials, CRC Press, Boca Raton, 2016.
[52] K.L. Scrivener, B. Lothenbach, N. De Belie, E. Gruyaert, J. Skibsted, R. Snellings, A. Vollpracht, TC 238-SCM: hydration and microstructure of concrete with SCMs, Mater. Struct. 48 (2015) 835–862.
[53] P.T. Durdziński, M.B. Haha, S.A. Bernal, N. De Belie, E. Gruyaert, B. Lothenbach, E. M. Méndez, J.L. Provis, A. Schöler, C. Stabler, Outcomes of the RILEM round robin on degree of reaction of slag and fly ash in blended cements, Mater. Struct. 50 (2017) 135.
[54] J.L. Poole, K.A. Riding, K.J. Folliard, M.C. Juenger, A.K. Schindler, Methods for calculating activation energy for Portland cement, ACI Mater. J. 104 (2007) 303–311.
[55] F. Ridi, E. Fratini, F. Mannelli, P. Baglioni, Hydration process of cement in the presence of a cellulosic additive.A calorimetric investigation 109 (2005) 14727–14734.
[56] L. D'aloia, G. Chanvillard, Determining the "apparent" activation energy of concrete: Ea—numerical simulations of the heat of hydration of cement, Cem. Concr. Res. 32 (2002) 1277–1289.
[57] S. Swaddiwudhipong, D. Chen, M. Zhang, Simulation of the exothermic hydration process of Portland cement, Adv. Cem. Res. 14 (2002) 61–69.
[58] J.J. Thomas, A new approach to modeling the nucleation and growth kinetics of tricalcium silicate hydration, J. Am. Ceram. Soc. 90 (2007) 3282–3288.
[59] J.J. Thomas, S. Ghazizadeh, E. Masoero, Kinetic mechanisms and activation energies for hydration of standard and highly reactive forms of β-dicalcium silicate (C2S), Cem. Concr. Res. 100 (2017) 322–328.
[60] S. Joseph, S. Uppalapati, O. Cizer, Instantaneous activation energy of alkali activated materials 3 (2018) 121–123.
[61] A. Fernández-Jiménez, F. Puertas, Alkali-activated slag cements: kinetic studies, Cem. Concr. Res. 27 (1997) 359–368.
[62] A.C.A. Muller, Characterization of porosity & CSH in cement pastes by 1H NMR, EPFL, 2014.
[63] B. Lothenbach, F. Winnefeld, C. Alder, E. Wieland, P. Lunk, Effect of temperature on the pore solution, microstructure and hydration products of Portland cement pastes, Cem. Concr. Res. 37 (2007) 483–491.
[64] K. De Weerdt, M.B. Haha, G. Le Saout, K. Kjellsen, H. Justnes, B. Lothenbach, The effect of temperature on the hydration of composite cements containing limestone powder and fly ash, Mater. Struct. 45 (2012) 1101–1114.
[65] B. Lothenbach, T. Matschei, G. Möschner, F.P. Glasser, Thermodynamic modelling of the effect of temperature on the hydration and porosity of Portland cement, Cem. Concr. Res. 38 (2008) 1–18.
[66] V. Kocaba, in: Development and evaluation of methods to follow microstructural development of cementitious systems including slags, Faculté Sciences et Techniques de l'Ingenieur, Ecole Polytechnique Fédérale de Lausanne, Lausanne, 2009, p. 263.
[67] D. Jansen, F. Goetz-Neunhoeffer, B. Lothenbach, J. Neubauer, The early hydration of ordinary Portland cement (OPC): an approach comparing measured heat flow with calculated heat flow from QXRD, Cem. Concr. Res. 42 (2012) 134–138.
[68] A. Quennoz, K.L. Scrivener, Hydration of C3A–gypsum systems, Cem. Concr. Res. 42 (2012) 1032–1041.
[69] F. Zunino, K. Scrivener, The influence of the filler effect on the sulfate requirement of blended cements, Cem. Concr. Res. 126 (2019), 105918.
[70] B. Lothenbach, G.Le Saout, M.B. Haha, R. Figi, E. Wieland, Hydration of a low-alkali CEM III/B–SiO2 cement (LAC) 42 (2012) 410–423.
[71] X. Feng, E.J. Garboczi, D.P. Bentz, P.E. Stutzman, T.O. Mason, Estimation of the degree of hydration of blended cement pastes by a scanning electron microscope point-counting procedure, Cem. Concr. Res. 34 (2004) 1787–1793.
[72] I.G. Richardson, Tobermorite/jennite- and tobermorite/calcium hydroxide-based models for the structure of C-S-H: applicability to hardened pastes of tricalcium silicate, β-dicalcium silicate, Portland cement, and blends of Portland cement with blast-furnace slag, metakaolin, or silica fume, Cem. Concr. Res. 34 (2004) 1733–1777.
[73] L. Nicoleau, A. Nonat, D. Perrey, The di- and tricalcium silicate dissolutions, Cem. Concr. Res. 47 (2013) 14–30.
[74] A.M. Gajewicz-Jaromin, P.J. McDonald, A.C. Muller, K.L. Scrivener, Influence of curing temperature on cement paste microstructure measured by 1H NMR relaxometry, Cem. Concr. Res. 122 (2019) 147–156.
[75] F. Avet, K. Scrivener, Effect of temperature on the water content of CASH in plain Portland and blended cements, Cem. Concr. Res. 136 (2020), 106124.
[76] R.B. Perkins, C.D. Palmer, Solubility of ettringite (Ca6 [Al (OH) 6] 2 (SO4) 3· 26H2O) at 5–75 C, Geochim. Cosmochim. Acta 63 (1999) 1969–1980.
[77] L. Divet, R. Randriambololona, Delayed ettringite formation: the effect of temperature and basicity on the interaction of sulphate and CSH phase, Cem. Concr. Res. 28 (1998) 357–363.
[78] R. Barbarulo, H. Peycelon, S. Leclercq, Chemical equilibria between C-S–H and ettringite, at 20 and 85 C, Cem. Concr. Res. 37 (2007) 1176–1181.
[79] B. Lothenbach, A. Nonat, Calcium silicate hydrates: solid and liquid phase composition, Cem. Concr. Res. 78 (2015) 57–70.
[80] E. L'Hôpital, B. Lothenbach, G. Le Saout, D. Kulik, K. Scrivener, Incorporation of aluminium in calcium-silicate-hydrates, Cem. Concr. Res. 75 (2015) 91–103.
[81] M. Merlini, G. Artioli, T. Cerulli, F. Cella, A. Bravo, Tricalcium aluminate hydration in additivated systems.A crystallographic study by SR-XRPD 38 (2008) 477–486.
[82] R. Snellings, G. Mertens, Ö. Cizer, J. Elsen, Early age hydration and pozzolanic reaction in natural zeolite blended cements: reaction kinetics and products by in situ synchrotron X-ray powder diffraction, Cem. Concr. Res. 40 (2010) 1704–1713.